# A dark matter telescope probing the 6 to 60 GHz band

Journal of Cosmology and Astroparticle Physics
An IOP and SISSA journal

# A dark matter telescope probing the 6 to 60 GHz band

**Javier De Miguel**

Instituto de Astrofísica de Canarias,
E-38200 La Laguna, Tenerife, Spain
Departamento de Astrofísica, Universidad de La Laguna,
E-38206 La Laguna, Tenerife, Spain

E-mail: jmiguel@iac.es

Received May 11, 2020
Revised December 1, 2020
Accepted February 9, 2021
Published April 28, 2021

**Abstract.** In this article we present the Dark-photons&Axion-Like particles Interferometer (DALI), a novel experiment designed for the detection of photon-mixing cold dark matter in the microwave band between 6 and 60 GHz. DALI is a haloscope for the simultaneous search for axions, axion-like particles and dark photons, with a number of novelties that make it unique. First, it is a dark matter telescope, with a capacity for pointing, tracking and rastering objects and areas in the sky. This potentially allows one to detect relativistic dark matter particles, substructures and flows, without compromising the simultaneous scanning for dark matter relic particles present in the laboratory. Second, it has been designed using commercial technology. This will allow feasible manufacture at a reasonable cost, thereby mitigating the need for R&D and facilitating maintenance. Finally, it benefits from a high sensitivity over a broad band of frequencies with only minimal reconfiguration.

**Keywords:** axions, dark matter detectors, dark matter experiments, gravitational waves / experiments

**ArXiv ePrint:** 2003.06874



https://doi.org/10.1088/1475-7516/2021/04/075

JCAP04(2021)075

## Contents



## 1 Introduction

One of the most important challenges of modern physics is to unveil the exact nature and properties of dark matter (DM). One of the leading hypotheses is that DM is composed of a new type of scalar particle, generically referred as the *axion*. The axion is a hypothetical pseudo-scalar Goldstone boson theorized by Weinberg and Wilczek [1, 2] as consequence of the dynamic solution to the *strong CP symmetry problem*[1] proposed by Peccei and Quinn (PQ) [3] and is predicted in multiple extensions of the Standard Model (SM) of Particle Physics. A fundamental parameter of the SM, the $\theta$ term, governs the value of the electric dipole moment of the neutron, and its absolute upper limit has been measured showing that $\theta$ is extremely fine tuned ($|\theta| < 10^{-11}$). In the PQ solution, $\theta$ is not a parameter but a dynamic field (the QCD axion[2]), whose potential has a minimum to which it evolves once the Universe cools sufficiently. The axion has a light mass, induced by its interactions with SM particles and scales inversely to a typical energy called the PQ scale, $f_a$. On the other hand, numerous extensions of the SM and String theory predict a set of particles similar to axion, the so-called *axion-like particles* or ALPs. The fundamentals of both QCD axion and ALPs have been adequately reviewed by several authors and the bibliography is very extensive (e.g., [4, 5]). Throughout this section, we focus only on those aspects which are relevant for the understanding of the present experiment, starting with the mechanism of interaction between axions and ALPs with ordinary photons. The axion-to-photon coupling Lagrangian density is

$$\mathcal{L} = -\frac{1}{4}F_{\mu\nu}F^{\mu\nu} + \frac{1}{2}\partial_\mu a\,\partial^\mu a - \frac{1}{2}m_a^2\,a^2 - \frac{g_{a\gamma}}{4}F_{\mu\nu}\tilde{F}^{\mu\nu}\,a - J^\mu A_\mu\,, \tag{1.1}$$

where $F^{\mu\nu}$ is the field strength tensor and $\tilde{F}$ is the dual field strength, $g_{a\gamma}$ is the axion-to-photon coupling constant, $a$ the axion field, $m_a$ the axion mass, $J$ is density of current and the SM photon field is $A^\mu$.

[1] Charge and Parity or Charge-conjugation Parity symmetry, i.e., charge conjugation symmetry (C) and parity symmetry (P).

[2] QCD stands for Quantum Chromodynamics.



JCAP04(2021)075

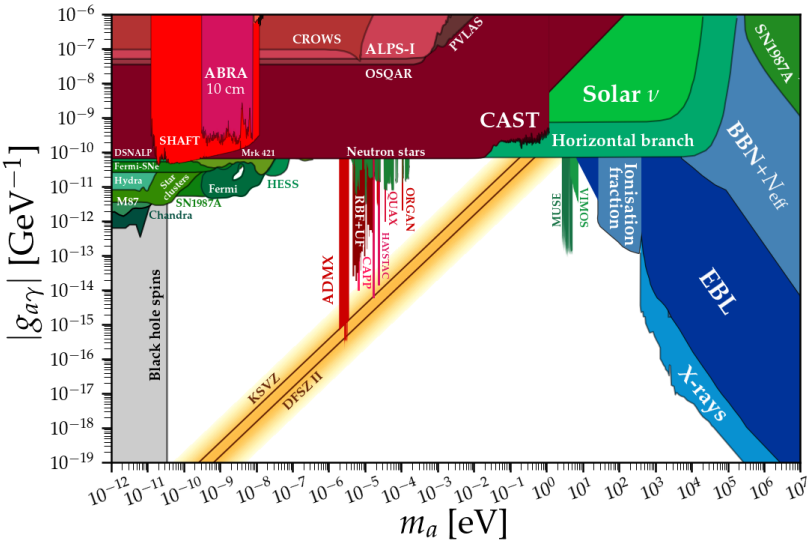


**Figure 1**. Exclusion graph of axion mass (log-scale). Laboratory experiments partially overlapping helioscopes are shaded in reddish colors. Greenish exclusion sectors are established by stellar hints and astronomical observations. Zones shaded in bluish colors correspond cosmology. Haloscopes are also represented in red [6].

A set of astronomical observations and laboratory experiments constrain the range of values in which the axion and ALPs mass can exist (e.g., [7–9]). For $f_a$ scales of the order of $10^{12}$ GeV, or masses of the order of the $\mu$eV, the axion and ALPs are well-grounded candidates for cold dark matter (CDM). This is represented in figure 1 where the (upper) reddish zones correspond to laboratory results, including *Light shining through walls* (LSW) experiments [10], measurement of axion-field induced dichroism and birefringence and vacuum magnetic birefringence (VMB) [11] and *Fifth force* experiments [12] partially overlapping *helioscopes* [13–15] and bounds depending on interactions (i.e., Primakoff [16] axion loss rate, atomic axio-recombination or deexcitaction, axion bremsstrahlung and Compton scattering interactions) of the axion to fermions and photons in the plasma of stars, producing extra cooling [17, 18], in green. The analysis includes observations of horizontal branch (HB) stars [19], red giants (RGs) [20], white dwarfs (WDs) [21], observations of the neutrino flux duration from supernova SN1987A compared to numerical simulations [22, 23], the neutron star (NS) in the SN remnant Cassiopeia A [24–27] and superradiance because of the formation of gravitationally bound states in black holes (BH) [28]. The search for axion in the range $10^{-6} \lesssim m_a \lesssim 10^{-3}$ is well-motivated [4]. Haloscopes are the most sensitive detectors within this range. Thus, the most sensitive reddish regions in figure 1 represent exclusion zones from haloscopes [29–36]. Cosmological arguments on cosmic microwave background (CMB), X and $\gamma$ rays, Big Bang nucleonsynthesis (BBN), cosmological extragalactic background light (EBL) and $\chi_{ion}$ considerations [37] are contained in the bluish sectors. Regarding the lower limit for axion mass, several authors suggest that ultra-light axions should not exist below $m_a \gtrsim 10^{-21}$–$10^{-22}$ eV (e.g., [38, 39]).

The coupling rate of the QCD axion contains a factor derived from the model-dependent ratio of electromagnetic (EM) and color anomalies ($\mathcal{E}/\mathcal{C}$) given by $C_{a\gamma} = 1.92(4) - \mathcal{E}/\mathcal{C}$,[3] being $C_{a\gamma} = -\frac{\alpha}{2\pi} g_{a\gamma} f_a$.[4] The color anomaly is an integer, and is also referred to in cosmology as the *domain wall number* (i.e., $\mathcal{C} \equiv \mathcal{N}_{DW}$). In the case of the KSVZ (Kim-Shifman-Vainshtein-

[3] Giving the number in brackets account on the uncertainty.
[4] Where $\alpha = e^2/4\pi$ is the dimensionless *fine structure constant*, $e$ being the *elementary charge*.



JCAP04(2021)075

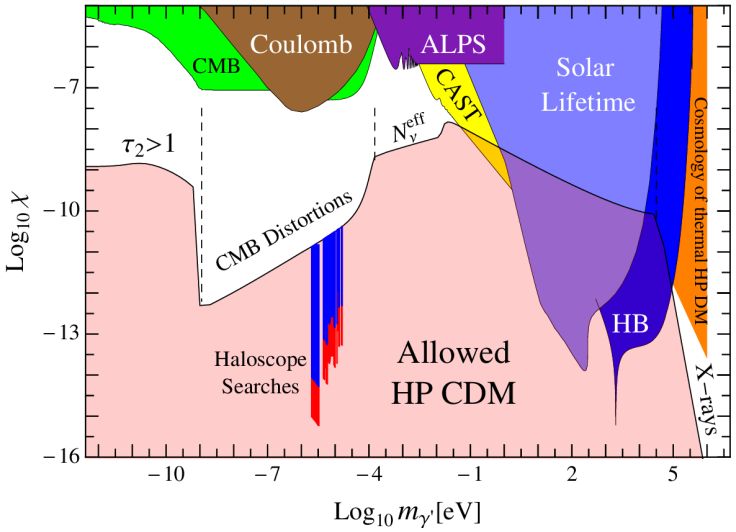


**Figure 2**. Exclusion graph for dark photon mass. Several experiments, astronomical bounds and cosmological considerations are included. Reprinted with permission from [37].

Zakharov) model [40, 41] $\mathcal{E}/\mathcal{N}_{DW} = 0$ and $\mathcal{N}_{DW} = 1$ are adopted. $\mathcal{N}_{DW} = 1$ avoids topological issues. Topological defects would have catastrophic cosmological effects if stable, so the KSVZ model is consistent. The DFSZ (Dine-Fischler-Srednicki-Zhitnitsky) model [42, 43] sets $\mathcal{E}/\mathcal{N}_{DW}$ equal 8/3 or 2/3 and $\mathcal{N}_{DW}$ equal to 6 or 3.[5] Alternative mechanisms to solve topology defects in DFSZ model have been proposed (e.g., [44]).

The *PQ-phase transition* is the moment in the history of the early universe in which the axion angular field acquires propagating degrees of freedom. In the pre-inflationary scenario an axion mass of the order of $m_a \lesssim 20\,\mu$eV is preferred. In the post-inflationary scenario different patches can have different misalignment angle $\theta_i$. These patches would remain causally disconnected and could give rise to the existence of DM substructures. This scenario undergoes the formation of cosmic strings and domain walls, solved when $\mathcal{N}_{DW} = 1$, as was mentioned above. Assuming that all (or a significant part of) the DM in the Universe has an axionic nature, and a DM halo density of the order of $\rho_{DM} \sim 300$–$450\,\mathrm{MeV\,cm^{-3}}$ [45], which will be adopted throughout the text, the value of the axion mass in this scenario is constrained in the range $26\,\mu eV \lesssim m_a \lesssim 1\,$meV.

Dark photon (DP), also called hidden photon or paraphoton [46, 47], arise in extensions of the SM. DPs naturally mix with SM photons. In the Lagrangian in eq. (1.2) we denote by $\tilde{X}^{\mu\nu}$ the field strength tensor of the DP field ($\tilde{X}^{\mu}$), and $F^{\nu\mu}$ the field strength tensor of the ordinary SM photon field ($A^{\mu}$) [48].

$$\mathcal{L} = -\frac{1}{4}F_{\mu\nu}F^{\mu\nu} - \frac{1}{4}\tilde{X}_{\mu\nu}\tilde{X}^{\mu\nu} - \frac{\chi}{2}F_{\mu\nu}\tilde{X}^{\mu\nu} + \frac{1}{2}m_{\gamma'}^2\,\tilde{X}_{\mu}\tilde{X}^{\mu} + J^{\mu}A_{\mu}\,, \tag{1.2}$$

where $\chi$ is the dimensionless kinetic mixing strength, $m_{\gamma'}$ the DP mass and $J^{\mu}$ the EM current density.

Dark photon is an interesting candidate for DM in the range $\chi \lesssim 10^{-11} - 10^{-10}$. The exclusion regions for DP are shown in figure 2. Details on the factors $\tau_2$, $N_\nu^{\mathrm{eff}}$, CMB Distortions and others can be consulted in [37].

[5] See DFSZI and DFSZII models.



JCAP04(2021)075

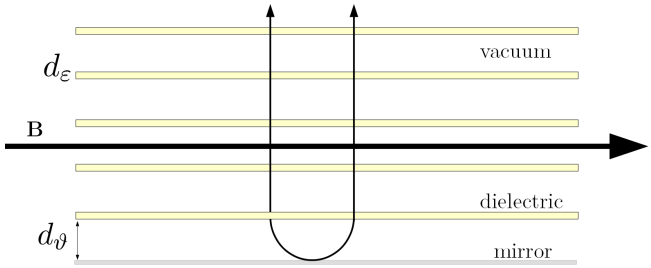


**Figure 3**. Experiment schematic. Axion-induced semi-plane waves are generated in the interface between vacuum and dielectric. The mirror at the bottom and a smart distribution of the plates can be used to create constructive interference. Consecutive plates act as a resonator producing power enhancement in a narrow band. The output can be received using microwave radiometers. The thickness between consecutive plates or between the bottom plate and the mirror ($d_\vartheta$) and the thickness of the dielectric plates ($d_\varepsilon$) must be adjusted with precision to maintain phase coherence.

In figure 1 it is remarkable that the region in the QCD axion sector $10^{-5} < m_a < 10^{-1}$ [eV] remains poorly explored. In figure 2 is shown an unexplored window for the detection of DPs. This experiment presents a potential to explore these sectors.

## 2 Experiment set-up

DALI was thought to operate in three different modes: *haloscope mode*, in which the instrument is stationary, and which focuses on the detection of relic axions forming part of the galactic halo; *tracking mode*, which benefits from the adding of an altazimuth platform that gives the detector the capacity of pointing and tracking sources on the sky; and *raster mode*, in which regions of the sky are covered with an algorithm that permits the scanning of wide areas searching for sources. Tracking and raster modes are *telescope mode*.

### 2.1 Theoretical foundation

The specific case of a dielectric interface surrounded by a vacuum within an external magnetic field shown in figure 3 is treated now. A modification of Maxwell's equations can be derived arising from a light, pseudo-stable QCD axion [49]. From a classical approach, the axion mix with photons within an EM field with a Lagrangian density

$$\mathcal{L}_{a\gamma} = \mathrm{g}_{a\gamma}\, a\, \mathrm{E}\cdot\mathrm{B}\ , \tag{2.1}$$

where E and B are the electric and magnetic field, respectively. Within the classic limit, the axion field can be approximated by $a = \theta_0 \cos(m_a t)\, f_a$, where $t$ is time and $\theta_0 \simeq 4\times10^{-19}$ [50].

Owing to the action of the magnetic field, a density current ($J$) enters on the right-hand side of Ampere's law in the interface between the vacuum and dielectric

$$J = -\mathrm{g}_{a\gamma}\, f_a\, \mathrm{B}\, \dot{\theta}\ , \tag{2.2}$$

where $\theta = \theta_0 \cos(m_a t)$. This generates an electric field (E) in the interface

$$\mathrm{E} = \int J\cdot ds = \frac{f_a}{\varepsilon}\, \mathrm{g}_{a\gamma}\, \mathrm{B}\, \theta(t)\ . \tag{2.3}$$

The application of continuity conditions to parallel boundaries in the interface between both media in eq. (2.3) ($\mathrm{E}_1 = \mathrm{E}_2$ & $\mathrm{B}_1 = \mathrm{B}_2$) shows that EM waves are generated to



JCAP04(2021)075

compensate for the discontinuity in electric permittivity ($\varepsilon_1 \neq \varepsilon_2$). Near the *zero velocity limit* of axions, the momentum parallel to the interface is conserved, whereas the perpendicular momentum is determined by the dispersion relations, forcing the EM waves to be emitted perpendicularly to the interface [51] with a frequency $\nu_a = m_a/2\pi$ [48].[6] A quantum-field theoretical derivation has been treated more recently for the same case of a planar dielectric interface surrounded by a vacuum, obtaining a similar result to that the used throughout this work [52].

The relation between $f_a$ and $m_a$ is (e.g., see [50])

$$m_a = 5.70(6)(4)\,\mu\text{eV}\frac{10^{12}\,\text{GeV}}{f_a}\,, \tag{2.4}$$

where the numbers in brackets account for the uncertainty.

The wavelength of EM radiation emitted from the surface is given by the axion oscillation pulse $\omega \sim m_a$. Thus

$$\lambda_a \simeq \frac{2\pi}{m_a}\,(\text{eV})(1.97\times10^{-7}\,\text{m})\,. \tag{2.5}$$

The calculation of the wavelength and mass relation of DPs is analogous to eq. (2.5).

### 2.2 Experimental approach

Several apparatus for axion and DP detection have been suggested. We highlight the dish-antenna [48, 53], cavity resonator haloscope [49] and Fabry-Pérot (FP) haloscope, including the so-called dielectric haloscope concept, adopted by the DALI experiment [54–56].[7] Experiments based on LC resonant circuits also present a remarkable potential for the search for ALPs, although they are generally shorter in bandwidth, limited to low frequencies and relatively weak in sensitivity.[8]

We have established the exclusion sectors for axion, ALPs and DP detection in figures 1 and 2. These graphics shown significant under-explored regions in both mass range or frequency and coupling strength. The origins of haloscopes are based on the need for power enhancement of the signal generated by axions and ALPs mixing with photons [49]. That is, the EM output produced by the physical mechanisms explained before in this manuscript is too weak owing to the limited magnetic inductance in real experiments (or low mixing strength, density) and must be enhanced before making possible a direct detection in a reasonable integration time.[9] In the pre-inflationary scenario, resonant cavity haloscopes are adequate. However, the dimensions of a resonant cavity scale with the wavelength, and cavity resonator haloscopes lose DB coherence when $m_a > 40\,\mu$eV [59], or they are too large in the radio-wave domain, where different set-ups are used (e.g., [60]). The post-inflationary mass range is accessible using FP haloscopes, and it is the aim of our experiment to explore this concept.[10]

In general, the principle of an FP interferometer is based on an interference between incoming and reflected waves within a resonator, forming a standing wave. Constructive

[6] Natural units are used throughout the text.

[7] Cavity resonator haloscopes are ongoing experiments.

[8] See [58] for a state-of-the-art proposal facing these limitations.

[9] Of the order of $10^{-27}\text{W/m}^2$ considering axions forming the galactic halo in the Solar System position [49] to be increased to around $10^{-23}\text{W/m}^2$.

[10] In the limit between pre- and post-inflationary scenarios, both resonant cavity and FP haloscopes can be used.



JCAP04(2021)075

interference occurs when incident and reflected waves are in phase. The output is spectrally modified compared to the input beam, allowing power enhancement in relatively narrow frequency bands centered at a resonant frequency. The classic FP resonator consists of a pair of mirrors surrounded by vacuum, or a medium with a known refractive index ($n = \sqrt{\varepsilon_r}$). FP interferometers and etalons have been used frequently in astronomy and are a very well established technology for infrared observations, where the mechanical requirements are relaxed compared to the optical range [61].

The classical theory on FP resonators has already been applied to the case of a dielectric (FP) haloscope [50, 62], where the *internal resonance enhancement factor* of the classic FP interferometer or the quality factor ($Q$) play a role in the so-called *boost factor* ($\beta$).[11] Throughout this work we follow this nomenclature. The boost factor is a figure of merit expressing the signal enhancement referred to a single magnetized mirror.[12] The power boost factor scales with the number of stacked plates (N) and its electric permittivity, $\beta^2(\nu, \mathrm{N}, \varepsilon_r)$. In the proof-of-concept experiments, a narrow fake axion signal is injected in a continuum, and then detected with $\sim 5\sigma$ significance using high-electron-mobility transistor (HEMT) radiometry [56, 63, 64].

Since DPs do not need the action of an external magnetic field to mix with SM photons, the observation of DPs maintains polarization coherence. In contrast, polarization in axion searching is degraded by the effects of the external magnetic field in haloscopes.

The DALI set-up is shown in figures 4 to 6. A multicoil superconducting magnet ("1") houses the FP interferometer and microwave receivers. Multicoil magnets are commonly used in magnetic resonance imaging (MRI), industry and research. They reach typical magnetic inductances of 3, 5, 7 and 9 T, and eventually higher. The bore size is typically around 0.5 m with magnetic-field lines parallel to the cylinder axis. In a regular model, the length of the coil winding part is around 1.5 m, while the magnet total length is about 2 m. Field homogeneity is typically 1% over a sphere of 100 mm diameter within the magnet bore and field stability is around 3 ppm/h. The superconducting magnet uses an independent helium free cooling system ("2"). The experiment cryostat ("3") is contained within the magnet's bore, but is independent. The cryostat is fabricated in non-magnetic material (Al).[13] In order to achieve high thermal stability and homogeneity, the cryostat is mounted symmetrically and equipped with twin cold-heads. The primary mirror is composed of a group of stacked dielectric parallel plates ("4"). These plates form the FP interferometer. A polished mirror is attached at the bottom ("5"). The dielectric plates are composed of a grid made of the union of commercial wafers. A higher electrical permittivity results in a higher signal power.[14] Standard dielectric wafers dimensions are 100 x 100 mm size of 0.25, 0.5, 0.75, 1 and 1.25 mm thicknesses. The polished surface roughness is around 0.02 $\mu$m. Each plate is mounted on a holder. Stacking wafers allows one to benefit from combining and intermediate thicknesses. This allows us to set a different plate thickness in every sub-band (or group of sub-bands) over the 6–60 GHz band, keeping $\beta^2$ not far from ideality. In order to benefit from maximum boost power, two thicknesses must be adjusted with precision: the plate spacing, which represents the thickness between consecutive plates or between the bottom plate and the mirror ($d_\vartheta$); and the thickness of the dielectric plates ($d_\varepsilon$). Both $d_\vartheta$ and $d_\varepsilon$ scale with wavelength. The theoretical thickness

[11] They differ by a factor that scales with the number of plates and its electric permittivity.

[12] Of area equal to the area of a plate, or equivalently the area of the mirror.

[13] Ti and fiberglass are also non-magnetic materials commonly used in cryogenics.

[14] We suggest to use zirconia ($ZrO_2$), a commercial material with dielectric constant $\varepsilon_r \simeq 29$ and loss tangent $\tan\delta \sim 10^{-4}$.



JCAP04(2021)075

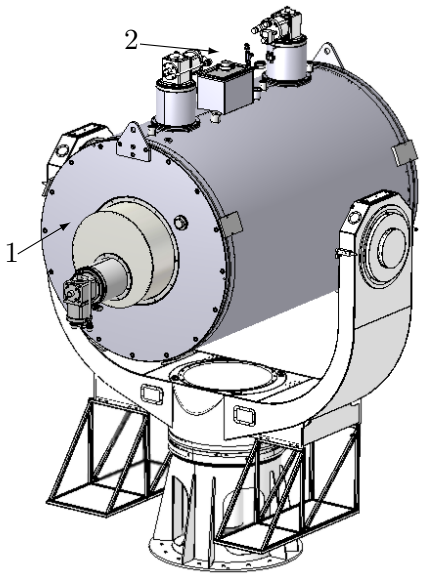


**Figure 4**. Experiment set-up. General view. DALI consist on a Fabry-Pérot interferometer within a cryostat. This cryostat is housed within a multicoil superconducting magnet ("1"). Approximate dimensions are 1.5x$\phi$1 m for the magnet and 2x$\phi$0.5 m of the experiment cryostat ("3").

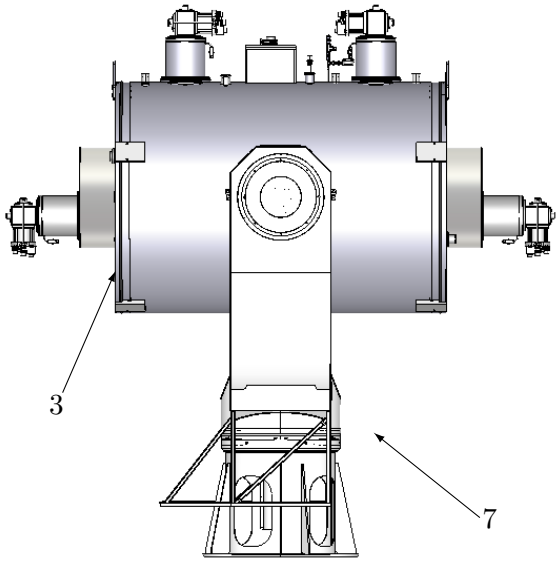


**Figure 5**. Experiment set-up. Lateral view. Symmetrical design allows one to improve the thermal stability for the experiment cryostat ("3"). The apparatus rests on an altazimultal mount ("7"), which permits pointing and tracking with high speed rotation. Some objects has been removed for simplicity.

of the dielectric plate $d_\varepsilon$ varies from around 2.5 mm at 6 GHz (or $m_a \sim$25 $\mu$eV) to 0.25 mm at 60 GHz (or $m_a \sim$250 $\mu$eV) when working near transparent mode. The vacuum thickness $d_\vartheta$ varies from around 25 mm at 6 GHz to 2 mm around 60 GHz. These have a remarkable consequence: since the dimensions of the magnet's bore are fixed, more dielectric plates can be stacked at higher frequencies, increasing the boost power. Thus, the instrument should be more sensitive at higher frequencies in the band, although there the quantum noise is also higher, compromising the benefit in sensitivity. To achieve a high boost factor, the sub-bands must be narrower at lower frequencies. The $\beta^2$ feature is narrow band because $P\Delta\nu_\beta$ is roughly constant. The plan is to scan in sub-bands of the order of $\Delta\nu_\beta \sim 100$ MHz wide, where $\beta^2 \sim 10^4$ is achievable in practice [55]. Since the sub-bands are determined before starting observations, a reliable optimal plate spacing can be calculated in advance using finite-element-method (FEM) 3D simulation.

For plate spacing, electro-mechanical actuators are used. Non-magnetic piezoelectric motors have been already proved in axion magnetized experiments [65, 66]. They present an uncertainty in the positioning of the order of $\pm 2$ $\mu$m. This uncertainty is in tension with the experiment's tolerance, of the order of a few $\mu$m at 60 GHz (and tens of $\mu$m at 6 GHz).[15] Static deflections and other systematic errors must be considered as well. However, part of the loss due to mechanical deviation would be absorbed by FP reconfiguration based on 3D-FEM EM simulations, in principle. The same logic is applicable to edge spurious effects and permittivity discontinuities in the dielectric grid, based on the results in [67] and [68].

[15] For 90% efficiency.



JCAP04(2021)075

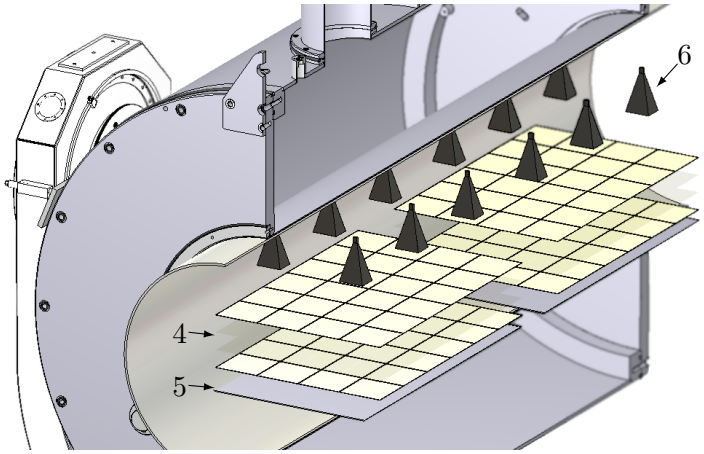


**Figure 6**. Experiment set-up. Section. Detail of resonator ("4" and "5") and antennas ("6"). The grid ("4") is resizable so that it can be adjusted to the de Broglie (DB) wavelength of the axion, acquiring coherence. Here a grid size for maximal sensitivity to virialized DM particles and accelerated particles up to velocities of the order of a few percent speed of light is shown.

Receivers can cover the focal plane of a telescope through different strategies. A classic schema incorporates a focusing mirror which concentrates all the photons in a reduced focal plane, and places a single detector that covers it completely. This is the case of reflector antennas [56, 69]. Differently, phased arrays [70] strategically place a number of antennas that cover a fraction of the focal plane each in order to combine their outputs. This is the case of focal plane arrays. This set-up has been used by numerous radio-telescopes over decades [71–75]. Both strategies are equivalent, ideally. Since sacrificing space within the magnet bore to incorporate a parabolic reflector would reduce the room available for plate stacking, DALI adopts the second configuration at the cost of introducing heavier electronics. Thus, the output power is received by an antenna array placed at the top of the cryostat ("6"). The signal is amplified in independent pixels using HEMTs[16] and processed in a cold front-end module. The signal is then transferred to a room-temperature back-end module, not shown in the schema for simplicity. The data acquisition system (DAS) is based on field-programmable gate array (FPGA) structure. The signal maintains phase coherence and the radiometer uses a pseudo cross-correlation schema. Cross-correlation allows one to mitigate the gain fluctuations (or equivalently noise temperature) by comparison between two uncorrelated signals [76]. A similar effect can be obtained by combining the signal from multiple outputs in a multi-receiver system. Hence, the mitigation of low frequency gain fluctuations caused by thermal and $1/f$ noise contributions is significant. Receivers could be pointed to cold-loads as a reference calibration signal, if necessary (e.g., see [77] and references therein). This might render the directional observation of relativistic axions possible, even in specific cases where the line width of the axion[17] (or DP) may be considerably wide, approaching $\Delta\nu_a/\nu \sim 1$ in extreme cases.

An altazimuth mount ("7") equipped with a rotating joint [78] transmits sufficient torque for fast rotation of the approximately 3 mT weight of the instrument, making pointing and tracking feasible.[18]

[16] We discuss an alternative technology in section 2.3.
[17] $\Delta\nu_a/\nu = \sigma^2_{v_a}/2$.
[18] The design shown in figure 4 is adapted from [73] and could undergo modifications.



JCAP04(2021)075

The experiment's laboratory must be isolated from spurious microwave backgrounds. A standard Faraday cage provides around 100–120 dB attenuation over 10 MHz and up to frequencies of tens of GHz.[19]

Since DM is weakly interactive, the telescope is bidirectional and some uncertainty in the pointing model is present. However, FP haloscopes are theoretically sensitive to the side of the plate in which the axion momentum is transferred trough phase information [79]. The line of sight (l.o.s.) of the instrument, perpendicular to the dielectric plates, bifurcates in l.o.s$^+$ and l.o.s$^-$ passing through the Earth. This allows simultaneous observation in both hemispheres.

### 2.3 Sensitivity projection

The sensitivity projection of DALI equipped with a 9 T multicoil superconducting magnet is shown in figure 8 for the specific configuration of interferometer presented in figure 6. In figure 8 we consider two different cases: (i) double stage $^3$He–$^4$He sorption cooler working with a background physical temperature of 1 K for HEMT based detectors [80] and a noise temperature consistent with the heat dissipation limit established by [81], or (ii) sub-kelvin operation replacing HEMTs with ultra-low-noise quantum devices [82–86].[20] The number of plates is given by N$\sim$ L$/(d_\varepsilon + d_\vartheta)$, where L is the length available for plate stacking inside the magnet bore, around 300 mm.[21] A study of the power boost factor incorporated to the estimate presented in figure 8 is included in figure 7, where 3D-FEM simulations are presented for a parsimonious[22] model of the interferometer. The group delay ($\tau_g$) informs on the mean lifetime of the photons within the interferometer in the resonant mode [87]. The quality factor of each individual cavity forming the interferometer scales as $Q = \omega \times \tau_g$ and the power boost factor around the resonant frequency is $\beta^2 \propto Q$. The boost factor scales linearly with the number of stacked plates ($\beta^2 \propto Q \propto$ N) [50]. Consequently, the boost varies between $\beta^2 \sim 10^{3-4}$ within the experimental range. Systematics are studied in [57, 63] and [64].

The sensitivity projection to relic axions and ALPs of DALI operating in haloscope mode over the entire 25 to 250 $\mu$eV range is shown in figure 8 (upper). The sensitivities are compared to theoretical predictions of reference axion models. In eqs. (2.6) to (2.8) $A$ is the collecting area, B the external field, $k_B$ the Boltzmann constant, $T_{\rm sys}$ the system temperature, $\Delta\nu \equiv \Delta\nu_a = 10^{-6}\nu$ the bandwidth referred to axion line width and $t$ is integration time. The axion-photon coupling factor is given by (e.g., see [50])

$$g_{a\gamma} = 2.04(3) \times 10^{-16}\, C_{a\gamma}\, \frac{m_a}{\mu\text{eV}}\,. \tag{2.6}$$

The axion-induced electric field generates an energy flux density [50, 62, 63]

$$\frac{P_{a\gamma}}{A} = 2.2 \times 10^{-27}\, \beta^2 \left(\frac{\text{B}}{10\,\text{T}}\right)^2 C_{a\gamma}^2 \left(\frac{\rho_{DM}}{0.3\,\text{GeVcm}^{-3}}\right)\,, \tag{2.7}$$

[19] Holland Shielding Systems BV, http://www.hollandshielding.com.

[20] The technology for ultra-low-noise detection involving high-frequencies is beyond the state-of-the-art.

[21] As $d_\vartheta \sim \lambda/2$, the most unfavorable frequency is 6 GHz, where 12 plates are stacked when working in transparent mode. A study is underway to determine if the plate spacing can be shortened without compromising the boost factor.

[22] Simplified, scaled, etc., whose results are transferable to the case of study.



JCAP04(2021)075

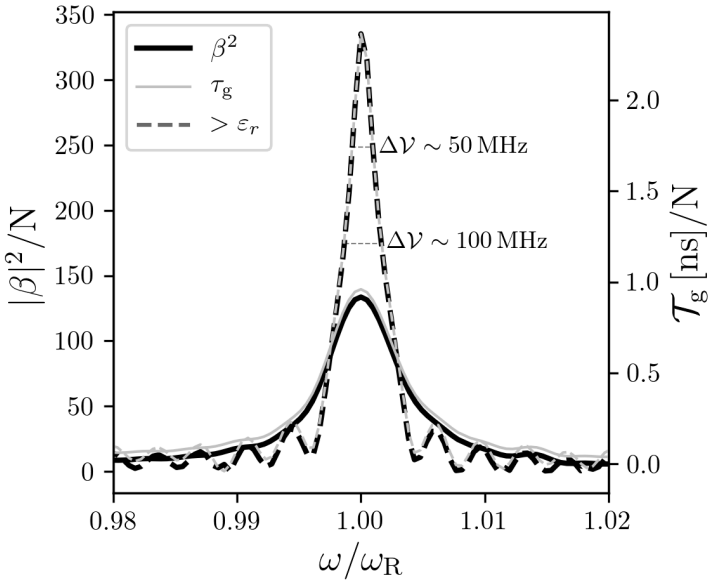


**Figure 7**. Power boost factor ($\beta^2$, in black) as a function of group delay time ($\tau_g$, in gray) around the resonant (pulse or equivalently) frequency ($\omega_R$) normalized to the number of stacked plates (N). Results from 3D-FEM simulations for a parsimonious model where $\varepsilon_r$= 9.4 ($Al_2O_3$, solid line) or 29 ($ZrO_2$, dashed line), $d_\varepsilon$=1 or 1.5 respectively, and $d_\vartheta \sim 7$ mm. A higher value of $\varepsilon_r$ results in a higher peak for $\beta^2$ ($\propto \varepsilon_r$) and a narrower full width at half maximum (FHWM) ($\propto \varepsilon_r^{-1}$). Two representative band widths ($\Delta\nu$) are highlighted as a reference for the estimate of the sensitivity of the experiment. The model is consistent with the experimental results presented in [56].

while the received power can be estimated using the well known *ideal radiometer equation* [90] in the form

$$\frac{S}{N} = \frac{P}{k_B\, T}\sqrt{\frac{t}{\Delta\nu}}\,. \tag{2.8}$$

The sensitivity to virialized DPs of the experiment over the 25–250 $\mu$eV band is shown in figure 8 (lower). In eq. (2.9) $\rho_{DM}$ is DM halo density, $A$ the detection area and $\alpha$ is a factor determining the incidence angle of the DP ($\alpha = \sqrt{2/3}$ represents random case) [48]. $P$ can be obtained from eq. (2.8) being $\Delta\nu \equiv \Delta\nu_{DP} = 10^{-6}\nu$.

$$\chi = 4.5\times 10^{-14}\left(\frac{P}{10^{-23}\,\mathrm{W}}\frac{0.3\,\mathrm{GeVcm^{-3}}}{\rho_{\mathrm{DM}}}\frac{\mathrm{m}^2}{\mathrm{A}}\frac{1}{\beta^2}\right)^{1/2}\frac{\sqrt{2/3}}{\alpha}\,. \tag{2.9}$$

The experiment shows a potential to probe unexplored axion (and ALPs) and DP sectors over a broad band of frequencies.

## 3 The aim for directional observation

The mathematical formalism and first approximations to establish a calculation of sensitivities for the case of low-velocity axions in stationary directional haloscopes have been elegantly carried out already in [51, 79]. Ongoing stationary low-frequency experiments incorporated some of these uncertainties some time ago, anticipating the possibility of receiving microwave



JCAP04(2021)075

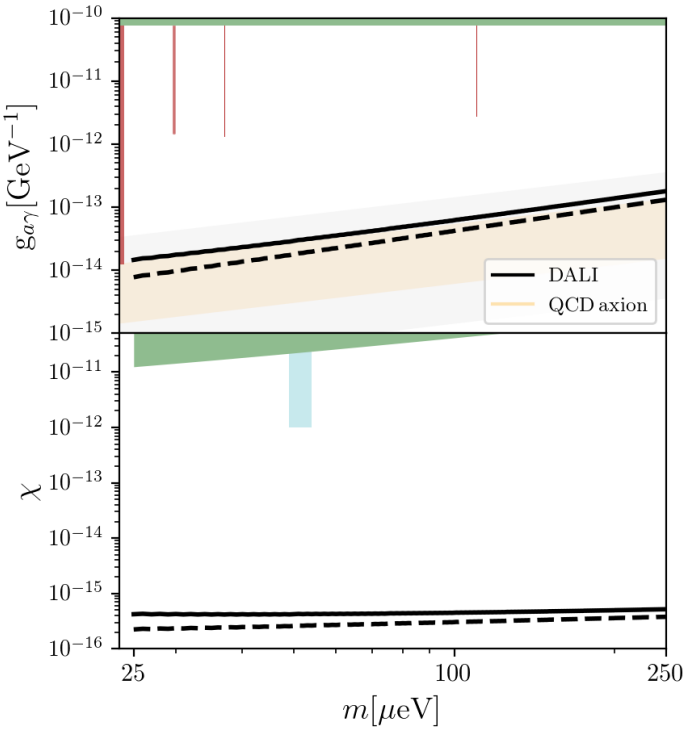


**Figure 8**. Sensitivity projection to relic axions (upper) and dark photons (lower) in the 6–60 GHz band. Parameters are B∼9 T, data are stacked over a few-month period by adding shortened integration times in order to make the experiment sensitive to the background modulation, $\rho_{DM} \sim 0.45\,\mathrm{GeVcm}^{-3}$, $\alpha$ corresponds to random velocity dispersion, $3\sigma$ significance and $T_{\mathrm{sys}}$ present two different cases: $^3$He-$^4$He sorption cooler down to a physical temperature about 1 K and HEMTs with a noise temperature about 2–3 times the quantum limit (solid line); and a bath temperature of 50 mK with ultra-low noise quantum detectors with a characteristic noise temperature about 1.5 times the quantum limit (dashed line). Sensitivities are compared to QCD axion models over the entire 25–250 $\mu$eV range. Exclusions regions in the vicinity are represented in green for horizontal branch (HB) and haloscopes in red [32, 35, 36]. The Tokyo limit is shown in blue [88]. The axion-model window in light gray is defined in [89].

photons from random axion events [91–94]. Helioscopes can be reconfigured in order to be sensitive to streaming CDM axions and miniclusters [95]. On the other hand, the velocity distribution of the galactic DM halo cannot be ideally isotropic, so directionality could be relevant even at this basic level.

The potential of this experiment to explore several theories and hypothesis involving astrophysical axion sources or the existence of DM substructures, such as tidal-streams and mini-clusters, in a 100% compatible and simultaneous mode to the conventional search for virialized axions forming the galactic-halo performed by classic haloscopes, relies on the aspects treated throughout this section.

### 3.1 Detectability of non-virialized particles

The velocity dispersion from the zero velocity limit up to the virial velocity around $10^{-3}$ through its effects on $\beta^2$ has been studied in a similar haloscope concept [51]. The detector becomes sensitive to velocity dispersion when the haloscope size is of the order of 15–20% of the axion DB wavelength. Below this limit, $\beta^2$ can in principle be considered velocity



JCAP04(2021)075

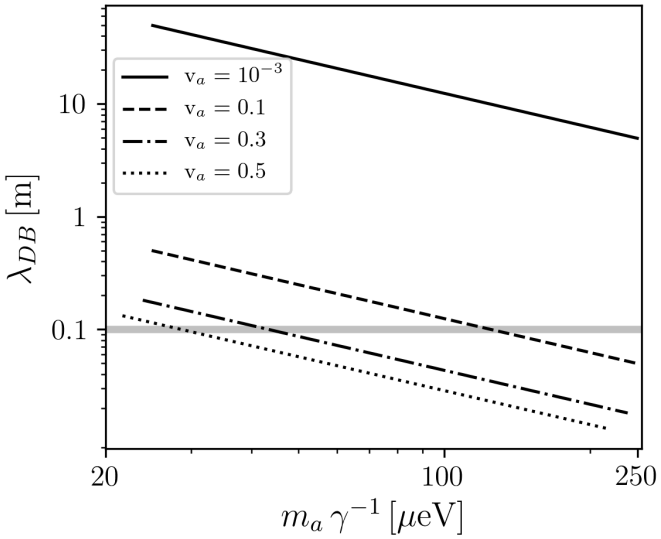


**Figure 9**. Study of de Broglie (DB) coherence in the frequency range 6–60 GHz. Limiting velocity ($v_{a_\ell}$) over mass of detectable axions. The gray horizontal line represents the limiting DB wavelength, which is coherent with a basic unit with $\ell \sim 0.1$ m. The region below the gray horizontal line loses DB coherence and is hidden. Axions with velocities up to around $0.5c$ are theoretically detectable with the more basic unit of grid of 10 cm length ($\ell = 0.1$). The virial velocity of the relic axions, around $10^{-3}c$, as reference, and relativistic velocities up to $0.5c$, are represented.

independent and so the instrument presents low or null sensitivity to velocity dispersion and incoming direction of the axion. When the DB wavelength of the axion is of the order of the size of the haloscope, directional sensitivity is $\mathcal{O}(1)$. This gives a strong directionality to the *axioscope*. Virialized axion search is weakly sensitive to directionality up to around 250 $\mu$eV.

The case of faster particles requires further analysis. The DB coherence must be maintained in order to make the axion detectable because of *cross-section* considerations.[23] Therefore, the DB wavelength of the axion or ALP ($\lambda_{DB} = 2\pi\gamma/m_a v_a$)[24] must be larger than the *collector* or *primary mirror* scale length ($\ell$). This allows the axion field to be measured including phase information. Given this, the detector is coherent when the following condition is fulfilled

$$v_{a_\ell} \lesssim \frac{2\pi}{\gamma\, m_a\, \ell}(\text{eV})(1.97 \times 10^{-7}\,\text{m})\ . \tag{3.1}$$

The expression in eq. (3.1) establishes a limit to the velocity of non-virialized axions that is possible to receive with a telescope characterized by the scale length of its detector ($v_{a_\ell}$). The limiting velocity scales inversely to axion mass. This can be examined with the help of figure 9, where the horizontal gray line represents the experiment's limit in scale length, to be compared to the relativistic DB wavelength shown in ordinate axis. Note the sector above the 0.1 m characteristic length line, revealing that axion velocities up to around 50% of the velocity of light in vacuo are accessible in the case of the basic unit of around 10 cm in length.[25] Lighter (i.e., $m_a < 25\,\mu$eV) relativistic axions are shifted to the

[23] See [96] pp. 86–87 for an intuitive review of this fundamental issue.

[24] $\gamma = 1/\sqrt{1 - v^2/c^2}$ is the Lorentz factor.

[25] Several basic units that cover the entire longitudinal section of the bore can be placed if they are sufficiently separated in order not to interfere.



JCAP04(2021)075

experiment band. However, at these energies, Lorentz relativistic correction to the axion rest mass below 15% ($\gamma \lesssim 1.15$) remain moderate, specially considering the limited spectral resolution of a FD haloscope. Many basic plate units can be stacked and paired to form bigger and thicker collector areas. Some examples are the cases of 2, 5 and 10 paired basic units (a basic unit presents $\ell \sim 0.1$, as mentioned) with respective velocities of 25, 10 and 5% speed of light at $m_a \sim 25\,\mu$eV. The diffraction limit $\ell_d \sim \lambda_a$ does not conflict with the scale length throughout the experimental range, eluding significant diffraction on the resonator plates. Finally, a highly relativistic velocity would dramatically reduce the sensitivity of the experiment mainly due to its effect on the axion phase, affecting the coherence length [51]. A practical realisation designed to scan for relativistic axions would require a setup with a limited number of plates and so a lower power boost factor, forcing a larger integration time. This would limit the detectability of non-virialized particles to velocities of the order of a few tens percent the speed of light, except in specific cases of higher occupation number compared to the local DM density.

### 3.2 A telescopic search for axion

Telescopic search for non-virialized DM particles does not compromise the classical (stationary) exploration for galactic halo axions and DPs. Both necessarily take place simultaneously during scanning. Particles of diverse origin could mix. An extra population of DM particles with similar *dynamic* mass would only result in a signal enhancement and hence an enhanced significance of detection, so long as the DB coherence is maintained. This would allow the detector to access sensitivity sectors that were previously prohibited. A modulation of the background signal would also reveal the signature of DM. In this section we discuss several examples:

1. the existence and detectability of DM substructures is an interesting hypothesis arising from anomalous large-scale observations and simulations. Axion streams density would vary between 0.3–30% of local DM density ($\rho_{DM}$). Thus, they would be potentially detectable. Furthermore, streams would present a $10^6$ flux enhancement factor compared to the local DM density (i.e., $\rho_a \sim 10^6 \rho_{DM}$) once aligned in the Sun-Earth l.o.s. focusing low velocity axions at the Earth's position [97]. Moreover, streams may be enhanced by microlensing. Gravitational microlens caused by planets in the direction planet-Earth may provide $\rho_a \sim 10^6 \rho_{DM}$, or around $\rho_a \sim 10^4 \rho_{DM}$ in the case of the Moon [98]. Only once data are stacked during month-year periods planetary effects underlying streams would be revealed in broad band observations with shortened integration time. A different case of interest is the Galactic-center-Sun-Earth alignment, repeated annually. This effect would be enhanced every 8–9 years, when the Moon is aligned in the same l.o.s. Streaming DM could explain why both the terrestrial atmospheric ionisation and solar activity show dependence on the longitudinal position of the planets or lunar phase [99]. Referring now to small-scale substructures such as miniclusters, they could be disrupted forming tidal streams with flux density $\rho_a \sim 10\rho_{DM}$ [100]. Stream-crossing events may occur around 1 every 20 years with a few-day duration, so the probability of entering or leaving a DM minicluster during a measurement is small. However, miniclusters trapped by the Solar System during its formation [98], with $\rho_a \sim 10^5 \rho_{DM}$ and few-day events duration annually have been suggested. Such trapped substructures are within the observational bounds [101]. Refer to [102–113] for a general view on the status of *dark universe* research. The same



JCAP04(2021)075

concept on DM substructures and flows explained here for the case of axions and ALPs can be extended to the search for DPs,

2. recently, the ANITA experiment, dedicated to measuring isolated impulsive radio signals originating from cosmic ray showers reflected in the Antarctica ice, reported the detection of two anomalous events, which are not explainable by cosmic rays [114, 115]. An explanation strictly within the SM conflicts with other experiments and theory. Different arguments over the years depend on further investigations and/or tend to be in tension with data (e.g. [116–120]). The possibility of instrumental artifacts must not be discarded either. However, authors have recently suggested that these events could be explained in terms of resonance in the ionosphere by the axion–photon conversion mechanism induced by axion *flares* [121],

3. with reference to stellar physics, solar axions produced by the Primakoff effect are ultra-relativistic, emitted with keV-level energies and so are invisible for our experiment [14]. However, axion quark nugget (AQN) theory [122] suggests a mechanism for creating a significant population of axions in the solar corona released with velocities of 10–90% of the speed of light [123]. The mass relativistic corrections are moderate, so photons generated by AQN-induced axion mechanisms may be received in the microwave range. AQN-induced axions would mix with relic axions [124]. AQN-induced axions present flux density $\rho_a \sim 10^{-5}\rho_{DM}$ and typical velocity around $0.5c$. Linearity in velocity enhances the flux density of AQN-induced axions up to $\rho_a \sim 10^{-2}\rho_{DM}$ [125]. Benefit from microlensing and perhaps also the halo modulation amplification time dependent factor would be helpful in finding these DM particles [126–128]. The preferred mass for AQN-induced axions is $m_a \sim 100\,\mu$eV [129]. Low velocity gravitationally trapped axions produced by AQN mechanism have been also suggested [130].

It is remarkable that DM-halo axions, axion substructures, isolated impulsive axion-induced signals (i.e., flares) and AQN-induced axions and DPs might be simultaneously explored during observations. The detection of non-virialized particles is preferably directional. Note that from the dot product in eq. (2.1) it follows that the interaction is maximal when the axion incidence angle to a dielectric plane is perpendicular to the magnetic field, transmitting maximum momenta. Otherwise, the transmission is penalized by a factor $\cos\iota$, with $\iota$ the incidence angle, and the signal is reduced accordingly. The study of the signal modulation originated by random crossing events is an interesting case. Although the analysis in [79] is devoted to a stationary directional search for axion, it can be extended to the case of a telescopic exploration for dark matter substructures. Dominated by celestial mechanics, the measured signal would be sinusoidally modulated. The daily signal modulation caused by an axionic event with a velocity $\mathrm{V}_a$ can be expressed in terms of the modulation parameters $c_0, c_1$ and $\phi$ in the form

$$\cos\xi_a^{\mathcal{N},\mathcal{W},\mathcal{Z}} = \frac{\hat{\mathrm{e}}^{\mathcal{N},\mathcal{W},\mathcal{Z}} \cdot (\mathrm{V}_{\mathrm{lab}} - \mathrm{V}_a)}{|\mathrm{V}_{\mathrm{lab}} - \mathrm{V}_a|} \longleftarrow c_0 + c_1 \cos(\omega_d\, t + \phi)\,, \tag{3.2}$$

where $\omega_d = 2\pi/0.997$, $t$ is time expressed in days from January 1st and $\mathrm{V}_{\mathrm{lab}}$ stands for the lab velocity in laboratory coordinates. For the case of stationary haloscopes featuring directional sensitivity, rectangular lab coordinates $\mathcal{N}, \mathcal{W}, \mathcal{Z}$ are adequate. The modulation



JCAP04(2021)075

parameters are

$$\overbrace{b_0\cos\lambda_{\rm lab}}^{c_0^{\mathcal{N}}}-\overbrace{b_1\sin\lambda_{\rm lab}}^{c_1^{\mathcal{N}}}\cos(\omega_d\,t+\overbrace{\phi_{\rm lab}+\psi}^{\phi^{\mathcal{N}}})\,, \tag{3.3}$$

$$\overbrace{b_1}^{c_1^{\mathcal{W}}}\cos(\omega_d\,t+\overbrace{\phi_{\rm lab}+\psi-\pi}^{\phi^{\mathcal{W}}})\,, \tag{3.4}$$

$$\overbrace{b_0\sin\lambda_{\rm lab}}^{c_0^{\mathcal{Z}}}+\overbrace{b_1\cos\lambda_{\rm lab}}^{c_1^{\mathcal{Z}}}\cos(\omega_d\,t+\overbrace{\phi_{\rm lab}+\psi}^{\phi^{\mathcal{Z}}})\,, \tag{3.5}$$

where an offset is cancelled while $b_0=\sigma_3|\mathrm{V}_{\rm lab}-\mathrm{V}_a|^{-1}$, $b_1=(\sigma_1^2+\sigma_2^2)^{1/2}|\mathrm{V}_{\rm lab}-\mathrm{V}_a|^{-1}$ and $\psi=\tan^{-1}(\sigma_1/\sigma_2)-0.721\omega_d-\pi/2$. The factors $\sigma_1=(-0.055,0.494,-0.868)\cdot\Upsilon$, $\sigma_2=(-0.873,-0.445,-0.198)\cdot\Upsilon$, $\sigma_3=(-0.484,0.747,0.456)\cdot\Upsilon$ arise in the conversion into lab coordinates; with $\Upsilon=\mathrm{V}_\odot+v_\oplus\cos(\tau_y)(0.994,0.109,0.003)+v_\oplus\sin(\tau_y)(-0.052,0.494,-0.868)$ and $\tau_y=2\pi\,(t-79)/365$. Note that a west pointing haloscope is not sensitive to $b_0$.

The experiment in figure 6 is shown pointing $\mathcal{Z}$. Altazimuth coordinates can be used to express a telescope rotation. The pointing tensor is $\hat{\mathrm{e}}_{\delta,\varphi}=(\sin\delta\cos\varphi,\sin\delta\sin\varphi,\cos\delta)$, where $\delta$ and $\varphi$ are the declination angle and the azimuthal angle in lab spherical coordinates, respectively. The transformation $c_i^{\delta,\varphi}=\hat{\mathrm{e}}^{\delta,\varphi}\,c_i^{\mathcal{N},\mathcal{W},\mathcal{Z}}$ is obtained from multiplying by $\hat{\mathrm{e}}^{\delta,\varphi}$ in eq. (3.2). Aimed to illustrate the features of a telescopic scan for axion we include figure 10. Here, the detection significance[26] of a telescope measuring a head-on crossing event is compared with the case of a stationary dielectric haloscope, with directionality given only by its geometry [51]. The preferred direction varies with lab coordinates $(\lambda_{\rm lab},\phi_{\rm lab})$ and during a year, and can be tracked in order to enhance the signal modulation. Figure 10 shows that a telescopic scan is up to two times more significant. Interestingly, this result is independent from instrumental sensitivity, axion model and mass, substructure density, velocity and dispersion. We also estimate that our experiment presents a potential to detect head-on events with a QCD axion density about several tens the local DM density ($\rho_{DM}$) and a velocity dispersion $\mathcal{O}(10)\,\mathrm{kms}^{-1}$ with a $3\sigma$ significance over a few day integration time by measuring its daily modulation. A denser occupation number, a more favourable relative velocity between the lab and the flow or a lower dispersion would result in a higher confidence level.

## 4 Summary and conclusions

Axion detection would be one of the most important moments of the entire history of Science. Given the fruitless searches of other dark matter candidates [131] and the discovery in July 2012 of a Higgs-like boson [132, 133], the first fundamental particle of a scalar nature,[27] there is a renewed effort in the scientific community to characterize experimentally and find the axion in the parameter space in which this can simultaneously solve the mystery of dark-matter and the problem of CP symmetry of the strong interaction. This energy space is weak and requires ultra sensitive detectors. In order to face this challenge, the haloscope was proposed [49].

In this article, we have presented a pioneering halo-telescope of high sensitivity and remarkable simplicity able to probe the 25–250 $\mu$eV mass range. The proposed set-up has the advantage of simultaneously exploring axion-like particles and dark photon sectors during

[26] As defined in ref. [79].

[27] Notice that axion is a pseudo-scalar particle.



JCAP04(2021)075

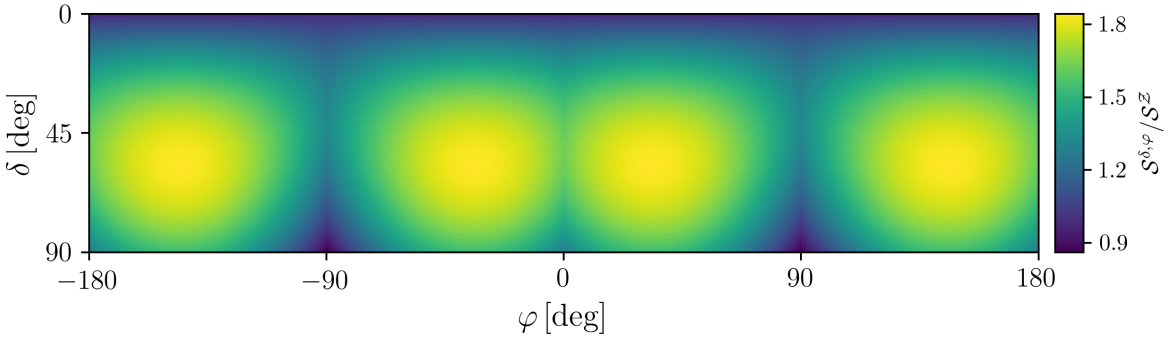


**Figure 10**. Significance of the signal modulation $\mathcal{S}^{\delta,\varphi}[\sigma]$ for a head-on axion event. Being $\delta$ the inclination angle measured from a fixed zenith direction ($\mathcal{Z}$), $\varphi$ the azimuthal angle of its orthogonal projection on a north-west ($\mathcal{N}-\mathcal{W}$) reference plane, measured from the north ($\mathcal{N}$) fixed reference. Full telescope rotation normalized to the signal modulation significance of a zenith pointing experiment ($\mathcal{S}^{z}[\sigma]$). Observed in the Canary Islands during the first day of the year.

scanning. A highlighted novelty of this experiment is the possibility of telescopic scanning. The apparatus is sensitive from low-velocity up to relativistic dark matter particles. The relevance on directionality and the exploration of non-virialized particles (astroparticles) is remarkable. The haloscope is the most sensitive instrument to date for the detection of relic axions, ALPs and dark photons. However, in the case that cold dark matter is distributed in the form of substructures (miniclusters, minihalos, etc.), and that Earth is placed within a low density region ($\rho_{\rm DM} \ll 300\,{\rm MeV\,cm^{-3}}$), haloscopes present a weakness since they depend on the local halo density. In this case, dark matter astroparticle scanning (assuming a significant particles flux) using telescopes and helioscopes, or laboratory experiments in which the axion pump is artificially generated, could be the only direct detection strategy. Note that heterogeneous populations are additive if they have a similar dynamic mass, resulting in an improved signal-to-noise ratio. On the other hand, mounting the detector on an altazimuth platform allows functionality to be added to the experiment at an assumable cost. *Axioastronomy* could probe several theories and hypotheses.[28]

Another remarkable advantage of the experiment is that it has been designed prioritizing the use of state-of-the-art (commercial) technology. The lack of the need for R&D reduces the cost in hardware and benefits from faster manufacturing and easier maintenance. On the other hand, the decision to use an (MRI type) commercial multicoil magnet, although this limits the size and the magnetic inductance that is possible to incorporate into the experiment, results in economy and reduced global fabrication time. We estimate that the cost of the experiment is reduced by an order of magnitude thanks to this strategy. That does not mean that the experiment could not benefit from the incorporation of incipient technologies.[29]

The experiment presents a potential to explore the QCD axion sector over the entire 6–60 GHz band sequentially, in sub-bands of the order of 100 MHz wide, each taking from a few weeks to several months of time for scanning, depending on the observational strategy and scan mode. In case of marginal detection, more time can be spent scanning the sub-band of interest. The reconfiguration needed for scanning the 6–60 GHz band is small and consists in grid resizing and the replacement of the microwave receivers.[30]

[28] See section 3 for an extended discussion.

[29] The MSA-based radiometer included in figure 8. Previously used in low frequency magnetized experiments, this technology might be feasible at higher frequencies.

[30] Standard radiometers have a typical bandwidth factor 1.4:1.



JCAP04(2021)075

Finally, graviton also mix with ordinary photons in the presence of external static magnetic fields [134, 135]. Cosmology predicts a stochastic gravitational wave background (GWB) generated by a number of mechanisms in the Universe.[31] Several experiments have been created to constraint the amplitude of the GWB in narrow bands, presenting a limited sensitivity [136–140]. The analysis carried out in [141] using data from the LSW experiments ALPS and OSQAR in [10, 142] and the CAST helioscope [14] establishes exclusion regions for the GWB of the order of $h_c \gtrsim 10^{-24} - 10^{-27}$ in several sub-bands in the THz and optic range, where $h_c$ represents the (dimensionless) minimum detectable characteristic amplitude of a stochastic, isotropic, stationary and unpolarized GWB. We explore the possibility that DALI might provide similar bounds for the GWB in the 6–60 GHz band.


## Acknowledgments

I would like to thank J. Martín Camalich and R. Rebolo for discussions. Thanks K. Zioutas, A. Zhitnitsky, J. Redondo, A. Sedrakian, E. Hernández and F. Gracia for comments.


## References


[1] S. Weinberg, *A new light boson?*, *Phys. Rev. Lett.* **40** (1978) 223 [INSPIRE].

[2] F. Wilczek, *Problem of Strong P and T invariance in the presence of instantons*, *Phys. Rev. Lett.* **40** (1978) 279 [INSPIRE].

[3] R.D. Peccei and H.R. Quinn, *CP conservation in the presence of instantons*, *Phys. Rev. Lett.* **38** (1977) 1440 [INSPIRE].

[4] Particle Data Group collaboration, *Review of particle physics*, *Phys. Rev. D* **98** (2018) 030001 [INSPIRE].

[5] D.J.E. Marsh, *Axion cosmology*, *Phys. Rept.* **643** (2016) 1 [arXiv:1510.07633] [INSPIRE].

[6] C. O'Hare, *Axionlimits*, Zenodo, (2020).

[7] L.F. Abbott and P. Sikivie, *A cosmological bound on the invisiblel axion*, *Phys. Lett. B* **120** (1983) 133 [INSPIRE].

[8] M. Dine and W. Fischler, *The not so harmless axion*, *Phys. Lett. B* **120** (1983) 137 [INSPIRE].

[9] J. Preskill, M.B. Wise and F. Wilczek, *Cosmology of the invisible axion*, *Phys. Lett. B* **120** (1983) 127 [INSPIRE].

[10] OSQAR collaboration, *New exclusion limits on scalar and pseudoscalar axionlike particles from light shining through a wall*, *Phys. Rev. D* **92** (2015) 092002 [arXiv:1506.08082] [INSPIRE].

[11] F. Della Valle et al., *The PVLAS experiment: measuring vacuum magnetic birefringence and dichroism with a birefringent Fabry–Perot cavity*, *Eur. Phys. J. C* **76** (2016) 24 [arXiv:1510.08052] [INSPIRE].

[12] G. Raffelt, *Limits on a CP-violating scalar axion-nucleon interaction*, *Phys. Rev. D* **86** (2012) 015001 [arXiv:1205.1776] [INSPIRE].

[13] D.M. Lazarus et al., *A search for solar axions*, *Phys. Rev. Lett.* **69** (1992) 2333 [INSPIRE].

[14] CAST collaboration, *New CAST limit on the axion-photon interaction*, *Nature Phys.* **13** (2017) 584 [arXiv:1705.02290] [INSPIRE].


[31] The coalescence of primordial black hole (PBH) binaries may produce a stochastic GWB component, while the evaporation of low-mass PBHs would produce high-frequency (MHz-GHz) GWs. These PBHs may be a DM component [145, 147]. *Branes* oscillation may be a different GWB component in the band $10^8$–$10^{14}$ Hz [146, 148]. The nucleosynthesis upper limit is $\Omega_{GW} \gtrsim 10^{-5}$ [149].



JCAP04(2021)075

[15] LUX collaboration, *First searches for axions and axionlike particles with the LUX experiment*, *Phys. Rev. Lett.* **118** (2017) 261301 [arXiv:1704.02297] [INSPIRE].

[16] H. Primakoff, *Photoproduction of neutral mesons in nuclear electric fields and the mean life of the neutral meson*, *Phys. Rev.* **81** (1951) 899 [INSPIRE].

[17] G.G. Raffelt, *Particle physics from stars*, *Ann. Rev. Nucl. Part. Sci.* **49** (1999) 163 [hep-ph/9903472] [INSPIRE].

[18] N. Vinyoles, A. Serenelli, F.L. Villante, S. Basu, J. Redondo and J. Isern, *New axion and hidden photon constraints from a solar data global fit*, *JCAP* **10** (2015) 015 [arXiv:1501.01639] [INSPIRE].

[19] I.G. Irastorza et al., eds., *Proceedings, 11th Patras workshop on axions, WIMPs and WISPs (Axion-WIMP 2015)*: Zaragoza, Spain, 22–26 June 2015, report number DESY-PROC-2015-02 Hamburg DESY (2015) [INSPIRE].

[20] N. Viaux et al., *Neutrino and axion bounds from the globular cluster M5 (NGC 5904)*, *Phys. Rev. Lett.* **111** (2013) 231301 [arXiv:1311.1669] [INSPIRE].

[21] M.M. Miller Bertolami, B.E. Melendez, L.G. Althaus and J. Isern, *Revisiting the axion bounds from the Galactic white dwarf luminosity function*, *JCAP* **10** (2014) 069 [arXiv:1406.7712] [INSPIRE].

[22] T. Fischer, S. Chakraborty, M. Giannotti, A. Mirizzi, A. Payez and A. Ringwald, *Probing axions with the neutrino signal from the next galactic supernova*, *Phys. Rev. D* **94** (2016) 085012 [arXiv:1605.08780] [INSPIRE].

[23] P. Carenza, T. Fischer, M. Giannotti, G. Guo, G. Martínez-Pinedo and A. Mirizzi, *Improved axion emissivity from a supernova via nucleon-nucleon bremsstrahlung*, *JCAP* **10** (2019) 016 [*Erratum ibid.* **05** (2020) E01] [arXiv:1906.11844] [INSPIRE].

[24] L.B. Leinson, *Axion mass limit from observations of the neutron star in Cassiopeia A*, *JCAP* **08** (2014) 031 [arXiv:1405.6873] [INSPIRE].

[25] J. Keller and A. Sedrakian, *Axions from cooling compact stars*, *Nucl. Phys. A* **897** (2013) 62 [arXiv:1205.6940] [INSPIRE].

[26] A. Sedrakian, *Axion cooling of neutron stars. II. Beyond hadronic axions*, *Phys. Rev. D* **99** (2019) 043011 [arXiv:1810.00190] [INSPIRE].

[27] M. Giannotti, I.G. Irastorza, J. Redondo, A. Ringwald and K. Saikawa, *Stellar recipes for axion hunters*, *JCAP* **10** (2017) 010 [arXiv:1708.02111] [INSPIRE].

[28] A. Arvanitaki, S. Dimopoulos, S. Dubovsky, N. Kaloper and J. March-Russell, *String axiverse*, *Phys. Rev. D* **81** (2010) 123530 [arXiv:0905.4720] [INSPIRE].

[29] ADMX collaboration, *A search for invisible axion dark matter with the axion dark matter experiment*, *Phys. Rev. Lett.* **120** (2018) 151301 [arXiv:1804.05750] [INSPIRE].

[30] S. De Panfilis et al., *Limits on the abundance and coupling of cosmic axions at 4.5-Microev < m(a) < 5.0-Microev*, *Phys. Rev. Lett.* **59** (1987) 839 [INSPIRE].

[31] W. Wuensch et al., *Results of a laboratory search for cosmic axions and other weakly coupled light particles*, *Phys. Rev. D* **40** (1989) 3153 [INSPIRE].

[32] HAYSTAC collaboration, *Results from phase 1 of the HAYSTAC microwave cavity axion experiment*, *Phys. Rev. D* **97** (2018) 092001 [arXiv:1803.03690] [INSPIRE].

[33] ADMX collaboration, *Piezoelectrically tuned multimode cavity search for axion dark matter*, *Phys. Rev. Lett.* **121** (2018) 261302 [arXiv:1901.00920] [INSPIRE].

[34] S. Lee, S. Ahn, J. Choi, B.R. Ko and Y.K. Semertzidis, *Axion dark matter search around 6.7 $\mu eV$*, *Phys. Rev. Lett.* **124** (2020) 101802 [arXiv:2001.05102] [INSPIRE].



JCAP04(2021)075

[35] B.T. McAllister, G. Flower, E.N. Ivanov, M. Goryachev, J. Bourhill and M.E. Tobar, *The organ experiment: an axion haloscope above 15 ghz*, *Phys. Dark Univ.* **18** (2017) 67.

[36] D. Alesini et al., *Galactic axions search with a superconducting resonant cavity*, *Phys. Rev. D* **99** (2019) 101101 [arXiv:1903.06547] [INSPIRE].

[37] P. Arias, D. Cadamuro, M. Goodsell, J. Jaeckel, J. Redondo and A. Ringwald, *WISPy cold dark matter*, *JCAP* **06** (2012) 013 [arXiv:1201.5902] [INSPIRE].

[38] B. Bozek, D.J.E. Marsh, J. Silk and R.F.G. Wyse, *Galaxy UV-luminosity function and reionization constraints on axion dark matter*, *Mon. Not. Roy. Astron. Soc.* **450** (2015) 209 [arXiv:1409.3544] [INSPIRE].

[39] D.J.E. Marsh and J. Silk, *A model for halo formation with axion mixed dark matter*, *Mon. Not. Roy. Astron. Soc.* **437** (2014) 2652 [arXiv:1307.1705] [INSPIRE].

[40] J.E. Kim, *Weak interaction singlet and strong CP invariance*, *Phys. Rev. Lett.* **43** (1979) 103 [INSPIRE].

[41] M.A. Shifman, A.I. Vainshtein and V.I. Zakharov, *Can confinement ensure natural CP invariance of strong interactions?*, *Nucl. Phys. B* **166** (1980) 493 [INSPIRE].

[42] M. Dine, W. Fischler and M. Srednicki, *A simple solution to the strong CP problem with a harmless axion*, *Phys. Lett. B* **104** (1981) 199 [INSPIRE].

[43] A.R. Zhitnitsky, *On possible suppression of the axion hadron interactions. (In russian)*, *Sov. J. Nucl. Phys.* **31** (1980) 260 [INSPIRE].

[44] S.M. Barr and J.E. Kim, *New confining force solution of the QCD axion Domain-Wall problem*, *Phys. Rev. Lett.* **113** (2014) 241301 [arXiv:1407.4311] [INSPIRE].

[45] E.I. Gates, G. Gyuk and M.S. Turner, *The local halo density*, *Astrophys. J. Lett.* **449** (1995) L123 [astro-ph/9505039] [INSPIRE].

[46] L. Okun, *The limits of electrodynamics - paraphotons*, *Zh. Eksp. Teor. Fiz.* **83** (1982) 892.

[47] A. Vilenkin, *Particles and the universe*, G. Lazarides and Q. Shafi (eds.), North Holland, Amsterdam (1986) p. 133.

[48] D. Horns, J. Jaeckel, A. Lindner, A. Lobanov, J. Redondo and A. Ringwald, *Searching for WISPy cold dark matter with a dish antenna*, *JCAP* **04** (2013) 016 [arXiv:1212.2970] [INSPIRE].

[49] P. Sikivie, *Experimental tests of the invisible axion*, *Phys. Rev. Lett.* **51** (1983) 1415 [*Erratum ibid.* **52** (1984) 695] [INSPIRE].

[50] A.J. Millar, G.G. Raffelt, J. Redondo and F.D. Steffen, *Dielectric haloscopes to search for axion dark matter: theoretical foundations*, *JCAP* **01** (2017) 061 [arXiv:1612.07057] [INSPIRE].

[51] A.J. Millar, J. Redondo and F.D. Steffen, *Dielectric haloscopes: sensitivity to the axion dark matter velocity*, *JCAP* **10** (2017) 006 [*Erratum ibid.* **05** (2018) E02] [arXiv:1707.04266] [INSPIRE].

[52] A.N. Ioannisian, N. Kazarian, A.J. Millar and G.G. Raffelt, *Axion-photon conversion caused by dielectric interfaces: quantum field calculation*, *JCAP* **09** (2017) 005 [arXiv:1707.00701] [INSPIRE].

[53] J. Jaeckel and S. Knirck, *Directional resolution of dish antenna experiments to search for WISPy dark matter*, *JCAP* **01** (2016) 005 [arXiv:1509.00371] [INSPIRE].

[54] G. Rybka, A. Wagner, A. Brill, K. Ramos, R. Percival and K. Patel, *Search for dark matter axions with the Orpheus experiment*, *Phys. Rev. D* **91** (2015) 011701 [arXiv:1403.3121] [INSPIRE].



JCAP04(2021)075

[55] MADMAX Working Group collaboration, *Dielectric haloscopes: a new way to detect axion dark matter*, *Phys. Rev. Lett.* **118** (2017) 091801 [arXiv:1611.05865] [INSPIRE].

[56] MADMAX collaboration, *A new experimental approach to probe QCD axion dark matter in the mass range above 40 μeV*, *Eur. Phys. J. C* **79** (2019) 186 [arXiv:1901.07401] [INSPIRE].

[57] S. Beurthey et al., *MADMAX Status Report*, arXiv:2003.10894 [INSPIRE].

[58] A.A. Melcón et al., *Axion searches with microwave filters: the RADES project*, *JCAP* **05** (2018) 040 [arXiv:1803.01243] [INSPIRE].

[59] I.G. Irastorza and J.A. Garcia, *Direct detection of dark matter axions with directional sensitivity*, *JCAP* **10** (2012) 022 [arXiv:1207.6129] [INSPIRE].

[60] J.L. Ouellet et al., *First results from ABRACADABRA-10 cm: a search for Sub-μeV Axion Dark Matter*, *Phys. Rev. Lett.* **122** (2019) 121802 [arXiv:1810.12257] [INSPIRE].

[61] M. R. Islam, M. M. Ali, M. H. Lai, K.-S. Lim, H. Ahmad, *Chronology of Fabry-Perot interferometer fiber-optic sensors and their applications: a review*, *Sensors* (Basel, Switzerland) 14 (2014) 7451.

[62] S. Knirck, *Madmax: a new way of probing qcd axion dark matter with a dielectric haloscope — foundations*, *J. Phys. Conf. Series* **1342** (2020) 012097.

[63] MADMAX Working Group collaboration, *MADMAX: a new dark matter axion search using a dielectric haloscope*, in *12th Patras Workshop on Axions, WIMPs and WISPs*, (2016) [arXiv:1611.04549] [INSPIRE].

[64] J. Egge, S. Knirck, B. Majorovits, C. Moore and O. Reimann, *A first proof of principle booster setup for the MADMAX dielectric haloscope*, *Eur. Phys. J. C* **80** (2020) 392 [arXiv:2001.04363] [INSPIRE].

[65] ADMX collaboration, *Piezoelectrically tuned multimode cavity search for axion dark matter*, *Phys. Rev. Lett.* **121** (2018) 261302 [arXiv:1901.00920] [INSPIRE].

[66] L. Zhong, B.M. Brubaker, S.B. Cahn and S.K. Lamoreaux, *Recent technical improvements to the HAYSTAC experiment*, *Springer Proc. Phys.* **211** (2018) 105 [arXiv:1706.03676] [INSPIRE].

[67] MADMAX collaboration, *Simulation studies for the MADMAX axion direct detection experiment*, in *14th Patras Workshop on Axions, WIMPs and WISPs*, (2018), arXiv:1811.00493 [INSPIRE].

[68] S. Knirck et al., *A first look on 3D effects in open axion haloscopes*, *JCAP* **08** (2019) 026 [arXiv:1906.02677] [INSPIRE].

[69] J. De Miguel-Hernández and R.J. Hoyland, *Fundamentals of horn antennas with low cross-polarization levels for radioastronomy and satellite communications*, 2019 *JINST* **14** R08001.

[70] R. Mailloux, *Phased array antenna handbook*, Artech House (1993), [ISBN10: 0890065020] [ISBN13: 9780890065020].

[71] R.A. Watson et al., *First results from the very small array. 1. Observational methods*, *Mon. Not. Roy. Astron. Soc.* **341** (2003) 1057 [astro-ph/0205378] [INSPIRE].

[72] A. Gregorio et al., *In-flight calibration and verification of the Planck-LFI instrument*, 2013 *JINST* **8** T07001 [arXiv:1307.2029] [INSPIRE].

[73] J.A. Rubino-Martin et al., *The QUIJOTE CMB experiment*, arXiv:0810.3141 [INSPIRE].

[74] GroundBIRD collaboration, *GroundBIRD : a CMB polarization experiment with MKID arrays*, *J. Low Temp. Phys.* **200** (2020) 384 [arXiv:2011.07705] [INSPIRE].



JCAP04(2021)075

[75] F. Incardona, *Observing the polarized cosmic microwave background from the earth: scanning strategy and polarimeters test for the LSPE/STRIP instrument*, Ph.D. Thesis, Milan University, (2020) arXiv:2009.01100 [INSPIRE].

[76] J. Faris, *Sensitivity of a correlation radiometer*, *J. of Research of the National Boreau of Standars C. Enginnering and Instrumentation* **71C** (1967).

[77] J. De Miguel-Hernández, R.J. Hoyland, M.F.G. Reñasco, J.A. Rubiño-Martín and T.A. Viera-Curbelo, *A high sensitivity fourier transform spectrometer for cosmic microwave background observations*, *IEEE Trans. Instrum. Measur.* **69** (2019) 4516 [arXiv:1910.10415] [INSPIRE].

[78] O. Tajima, J. Choi, M. Hazumi, H. Ishitsuka, M. Kawai and M. Yoshida, *GroundBIRD: an experiment for CMB polarization measurements at a large angular scale from the ground*, in: Millimeter, Submillimeter, and Far-Infrared Detectors and Instrumentation for Astronomy VI, *Proc. SPIE* **8452** (2012) 84521M.

[79] S. Knirck, A.J. Millar, C.A.J. O'Hare, J. Redondo and F.D. Steffen, *Directional axion detection*, *JCAP* **11** (2018) 051 [arXiv:1806.05927] [INSPIRE].

[80] M.A. McCulloch, J. Grahn, S.J. Melhuish, P.A. Nilsson, L. Piccirillo, J. Schleeh and N. Wadefalk, *Dependence of noise temperature on physical temperature for cryogenic low-noise amplifiers*, *J. Astron. Teles. Instr. Sys.* **3** (2017) 014003.

[81] J. Schleeh, J. Mateos, I. Íñiguez-de-la-Torre, N. Wadefalk, P.A. Nilsson, J. Grahn and A.J. Minnich, *Phonon black-body radiation limit for heat dissipation in electronics*, *Nature Mater.* **14** (2015) 187.

[82] J. Clarke, D. Kinion, *The microstrip SQUID amplifier: upgrading the axion dark matter experiment (ADMX)*, *Am. Phys. Soc.* California section meeting abstracts, (2011) p. F2.007.

[83] ADMX collaboration, *Design and performance of the ADMX SQUID-based microwave receiver*, *Nucl. Instrum. Meth. A* **656** (2011) 39 [arXiv:1105.4203] [INSPIRE].

[84] S. O'Kelley, G. Hilton, J. Clarke, ADMX Collaboration, *Tunable microstrip SQUID amplifiers for the Gen 2 Axion Dark Matter eXperiment (ADMX)*, *Am. Phys. Soc.*, April Meeting Abstracts, **2016** (2016) K16.004.

[85] S. Uchaikin et al., *Development of squid amplifiers for axion search experiments*, *2019 IEEE International Superconductive Electronics Conference (ISEC)* (2019) pp. 1–3.

[86] A. MATLAShov, M. Schmelz, V. Zakosarenko, R. Stolz and Y.K. Semertzidis, *SQUID amplifiers for axion search experiments*, *Cryogenics* **91** (2018) 125 [INSPIRE].

[87] K. Renk, *Basics of laser physics*, Springer, Berlin, Heidelberg (2012), pp. 45-46.

[88] J. Suzuki, Y. Inoue, T. Horie and M. Minowa, *Hidden photon CDM search at Tokyo*, in *11th Patras Workshop on Axions, WIMPs and WISPs*, (2015), [arXiv:1509.00785] [INSPIRE].

[89] L. Di Luzio, F. Mescia and E. Nardi, *Redefining the axion window*, *Phys. Rev. Lett.* **118** (2017) 031801 [arXiv:1610.07593] [INSPIRE].

[90] R.H. Dicke, *The measurement of thermal radiation at microwave frequencies*, *Sci. Inst.* **17** (1946) 268.

[91] L. Duffy, *High resolution search for dark matter axions in milky way halo substructure*, Ph.D. Thesis, Florida University (2006).

[92] L.D. Duffy and K. van Bibber, *Axions as Dark Matter Particles*, *New J. Phys.* **11** (2009) 105008 [arXiv:0904.3346] [INSPIRE].

[93] K. Choi, J. E. Kim, D. Son, *Proceedings on 11th international symposium on particles, strings and cosmology (PASCOS 2005)*, *AIP Conf. Proc.* **805** (2005) pp.1–486.



JCAP04(2021)075

[94] J. Hoskins et al., *Modulation sensitive search for nonvirialized dark-matter axions*, *Phys. Rev. D* **94** (2016) 082001 [arXiv:1804.08770] [INSPIRE].

[95] K. Zioutas et al., *Search for axions in streaming dark matter*, arXiv:1703.01436 [INSPIRE].

[96] A. Larkoski, *Elementary particle physics. An intuitive introduction*, Cambridge University Press (2019) pp.86–87 [ISBN:9781108496988].

[97] B.J. Patla, NIST, private communication (2017).

[98] K. Zioutas et al., *Search for axions in streaming dark matter*, arXiv:1703.01436 [INSPIRE].

[99] S. Bertolucci, K. Zioutas, S. Hofmann and M. Maroudas, *The Sun and its Planets as detectors for invisible matter*, *Phys. Dark Univ.* **17** (2017) 13 [arXiv:1602.03666] [INSPIRE].

[100] P. Tinyakov, I. Tkachev and K. Zioutas, *Tidal streams from axion miniclusters and direct axion searches*, *JCAP* **01** (2016) 035 [arXiv:1512.02884] [INSPIRE].

[101] J.M. Frere, F.-S. Ling and G. Vertongen, *Bound on the dark matter density in the solar system from planetary motions*, *Phys. Rev. D* **77** (2008) 083005 [astro-ph/0701542] [INSPIRE].

[102] P. Tinyakov, I. Tkachev and K. Zioutas, *Tidal streams from axion miniclusters and direct axion searches*, *JCAP* **01** (2016) 035 [arXiv:1512.02884] [INSPIRE].

[103] V.I. Dokuchaev, Y.N. Eroshenko and I.I. Tkachev, *Destruction of axion miniclusters in the Galaxy*, *J. Exp. Theor. Phys.* **125** (2017) 434 [arXiv:1710.09586] [INSPIRE].

[104] V.S. Berezinsky, V.I. Dokuchaev and Y.N. Eroshenko, *Formation and internal structure of superdense dark matter clumps and ultracompact minihaloes*, *JCAP* **11** (2013) 059 [arXiv:1308.6742] [INSPIRE].

[105] S. Davidson and T. Schwetz, *Rotating drops of axion dark matter*, *Phys. Rev. D* **93** (2016) 123509 [arXiv:1603.04249] [INSPIRE].

[106] I.I. Tkachev, *Fast radio bursts and axion miniclusters*, *JETP Lett.* **101** (2015) 1 [arXiv:1411.3900] [INSPIRE].

[107] M. Fairbairn, D.J.E. Marsh and J. Quevillon, *Searching for the QCD axion with gravitational microlensing*, *Phys. Rev. Lett.* **119** (2017) 021101 [arXiv:1701.04787] [INSPIRE].

[108] M. Fairbairn, D.J.E. Marsh, J. Quevillon and S. Rozier, *Structure formation and microlensing with axion miniclusters*, *Phys. Rev. D* **97** (2018) 083502 [arXiv:1707.03310] [INSPIRE].

[109] D.G. Levkov, A.G. Panin and I.I. Tkachev, *Gravitational Bose-Einstein condensation in the kinetic regime*, *Phys. Rev. Lett.* **121** (2018) 151301 [arXiv:1804.05857] [INSPIRE].

[110] L. Visinelli, S. Baum, J. Redondo, K. Freese and F. Wilczek, *Dilute and dense axion stars*, *Phys. Lett. B* **777** (2018) 64 [arXiv:1710.08910] [INSPIRE].

[111] C.J. Hogan and M.J. Rees, *Axion miniclusters*, *Phys. Lett. B* **205** (1988) 228 [INSPIRE].

[112] M. Vogelsberger and S.D.M. White, *Streams and caustics: the fine-grained structure of LCDM haloes*, *Mon. Not. Roy. Astron. Soc.* **413** (2011) 1419 [arXiv:1002.3162] [INSPIRE].

[113] S. Bertolucci, K. Zioutas, S. Hofmann and M. Maroudas, *The sun and its planets as detectors for invisible matter*, *Phys. Dark Univ.* **17** (2017) 13.

[114] ANITA collaboration, *Observation of an unusual upward-going cosmic-ray-like event in the third flight of ANITA*, *Phys. Rev. Lett.* **121** (2018) 161102 [arXiv:1803.05088] [INSPIRE].

[115] IceCube collaboration, *A search for IceCube events in the direction of ANITA neutrino candidates*, arXiv:2001.01737 [INSPIRE].

[116] K.D. de Vries and S. Prohira, *Coherent transition radiation from the geomagnetically-induced current in cosmic-ray air showers: Implications for the anomalous events observed by ANITA*, *Phys. Rev. Lett.* **123** (2019) 091102 [arXiv:1903.08750] [INSPIRE].



JCAP04(2021)075

[117] I.M. Shoemaker, A. Kusenko, P.K. Munneke, A. Romero-Wolf, D.M. Schroeder and M.J. Siegert, *Reflections on the anomalous ANITA events: the antarctic subsurface as a possible explanation*, *Annals Glaciol.* **61** (2020) 92 [arXiv:1905.02846] [INSPIRE].

[118] D.B. Fox et al., *The ANITA anomalous events as signatures of a beyond standard model particle, and supporting observations from IceCube*, arXiv:1809.09615 [INSPIRE].

[119] G.-y. Huang, *Sterile neutrinos as a possible explanation for the upward air shower events at ANITA*, *Phys. Rev. D* **98** (2018) 043019 [arXiv:1804.05362] [INSPIRE].

[120] J.M. Cline, C. Gross and W. Xue, *Can the ANITA anomalous events be due to new physics?*, *Phys. Rev. D* **100** (2019) 015031 [arXiv:1904.13396] [INSPIRE].

[121] I. Esteban, J. Lopez-Pavon, I. Martinez-Soler and J. Salvado, *Looking at the axionic dark sector with ANITA*, *Eur. Phys. J. C* **80** (2020) 259 [arXiv:1905.10372] [INSPIRE].

[122] A.R. Zhitnitsky, *'Nonbaryonic' dark matter as baryonic color superconductor*, *JCAP* **10** (2003) 010 [hep-ph/0202161] [INSPIRE].

[123] H. Fischer, X. Liang, Y. Semertzidis, A. Zhitnitsky and K. Zioutas, *New mechanism producing axions in the AQN model and how the CAST can discover them*, *Phys. Rev. D* **98** (2018) 043013 [arXiv:1805.05184] [INSPIRE].

[124] X. Liang and A. Zhitnitsky, *Gravitationally bound axions and how one can discover them*, *Phys. Rev. D* **99** (2019) 023015 [arXiv:1810.00673] [INSPIRE].

[125] P.W. Graham and S. Rajendran, *New observables for direct detection of axion dark matter*, *Phys. Rev. D* **88** (2013) 035023 [arXiv:1306.6088] [INSPIRE].

[126] J.D. Vergados and Y. Semertzidis, *Axionic dark matter signatures in various halo models*, *Nucl. Phys. B* **915** (2017) 10 [arXiv:1601.04765] [INSPIRE].

[127] S. Ge, H. Rachmat, M.S.R. Siddiqui, L. Van Waerbeke and A. Zhitnitsky, *X-ray annual modulation observed by XMM-Newton and Axion Quark Nugget Dark Matter*, arXiv:2004.00632 [INSPIRE].

[128] F. Froborg and A.R. Duffy, *Annual modulation in direct dark matter searches*, *J. Phys. G* **47** (2020) 094002 [arXiv:2003.04545] [INSPIRE].

[129] D. Budker, V.V. Flambaum, X. Liang and A. Zhitnitsky, *Axion quark nuggets and how a global network can discover them*, *Phys. Rev. D* **101** (2020) 043012 [arXiv:1909.09475] [INSPIRE].

[130] K. Lawson, X. Liang, A. Mead, M.S.R. Siddiqui, L. Van Waerbeke and A. Zhitnitsky, *Gravitationally trapped axions on the Earth*, *Phys. Rev. D* **100** (2019) 043531 [arXiv:1905.00022] [INSPIRE].

[131] M. Schumann, *Direct detection of WIMP dark matter: concepts and status*, *J. Phys. G* **46** (2019) 103003 [arXiv:1903.03026] [INSPIRE].

[132] ATLAS collaboration, *Observation of a new particle in the search for the standard model higgs boson with the ATLAS detector at the LHC*, *Phys. Lett. B* **716** (2012) 1 [arXiv:1207.7214] [INSPIRE].

[133] CMS collaboration, *Observation of a new boson at a mass of 125 GeV with the CMS Experiment at the LHC*, *Phys. Lett. B* **716** (2012) 30 [arXiv:1207.7235] [INSPIRE].

[134] M. Gertsenshtein, *Wave resonance of light and gravitational waves*, *JETP* **14** (1962) 84.

[135] J.A.R. Cembranos, M.C. Diaz and P. Martin-Moruno, *Graviton-photon oscillation in alternative theories of gravity*, *Class. Quant. Grav.* **35** (2018) 205008 [arXiv:1806.11020] [INSPIRE].

[136] HOLOMETER collaboration, *MHz gravitational wave constraints with decameter michelson interferometers*, *Phys. Rev. D* **95** (2017) 063002 [arXiv:1611.05560] [INSPIRE].



JCAP04(2021)075

[137] A.M. Cruise and R.M.J. Ingley, *A prototype gravitational wave detector for 100-MHz*, *Class. Quant. Grav.* **23** (2006) 6185 [INSPIRE].

[138] T. Akutsu et al., *Search for a stochastic background of 100-MHz gravitational waves with laser interferometers*, *Phys. Rev. Lett.* **101** (2008) 101101 [arXiv:0803.4094] [INSPIRE].

[139] A. Nishizawa et al., *Laser-interferometric detectors for gravitational wave background at 100 MHz: detector design and sensitivity*, *Phys. Rev. D* **77** (2008) 022002 [arXiv:0710.1944] [INSPIRE].

[140] A. Ito, T. Ikeda, K. Miuchi and J. Soda, *Probing GHz gravitational waves with graviton–magnon resonance*, *Eur. Phys. J. C* **80** (2020) 179 [arXiv:1903.04843] [INSPIRE].

[141] A. Ejlli, D. Ejlli, A.M. Cruise, G. Pisano and H. Grote, *Upper limits on the amplitude of ultra-high-frequency gravitational waves from graviton to photon conversion*, *Eur. Phys. J. C* **79** (2019) 1032 [arXiv:1908.00232] [INSPIRE].

[142] K. Ehret et al., *New ALPS results on hidden-sector lightweights*, *Phys. Lett. B* **689** (2010) 149 [arXiv:1004.1313] [INSPIRE].

[143] Y.B. Zeldovich, *Electromagnetic and gravitational waves in a stationary magnetic field* , *JETP* **65** (1973) 1311.

[144] D.V. Galtsov, Yu.V. Gratz and V.I. Petukhov *Radiation of gravitational waves by electrodynamic systems*, Moscow University (1984).

[145] G.S. Bisnovatyi-Kogan and V.N. Rudenko, *Very high frequency gravitational wave background in the universe*, *Class. Quant. Grav.* **21** (2004) 3347 [gr-qc/0406089] [INSPIRE].

[146] M. Servin and G. Brodin, *Resonant interaction between gravitational waves, electromagnetic waves and plasma flows*, *Phys. Rev. D* **68** (2003) 044017 [gr-qc/0302039] [INSPIRE].

[147] G. Bisnovatyi-Kogan and V. Rudenko, *Relativistic gravitation and gravitational radiation*, ed. J.A. Marck and J.P. Lasota, Cambridge University Press (1997), https://cds.cern.ch/record/308812.

[148] C. Clarkson and S.S. Seahra, *A gravitational wave window on extra dimensions*, *Class. Quant. Grav.* **24** (2007) F33 [astro-ph/0610470] [INSPIRE].

[149] M. Maggiore, *Gravitational wave experiments and early universe cosmology*, *Phys. Rept.* **331** (2000) 283 [gr-qc/9909001] [INSPIRE].

JCAP04(2021)075